Truncated Physical Model for Dynamic Sensor Networks with Applications in High-Resolution Mobile Sensing and BIGDATA

Thomas J. Matarazzo, S.M.ASCE[1]; and Shamim N. Pakzad, A.M.ASCE[2]

Abstract: Historically, structural health monitoring (SHM) has relied on fixed sensors, which remain at specific locations in a structural system throughout data collection. This paper introduces state-space approaches for processing data from sensor networks with time-variant configurations, for which a novel truncated physical model (TPM) is proposed. The state-space model is a popular representation of the second-order equation of motion for a multidegree of freedom (MDOF) system in first-order matrix form based on field measurements and system states. In this mathematical model, a spatially dense observation space on the physical structure dictates an equivalently large modeling space, i.e., more total sensing nodes require a more complex dynamic model. Furthermore, such sensing nodes are expected to coincide with state variable DOF. Thus, the model complexity of the underlying dynamic linear model depends on the spatial resolution of the sensors during data acquisition. As sensor network technologies evolve and with increased use of innovative sensing techniques in practice, it is desirable to decouple the size of the dynamic system model from the spatial grid applied through measurement. This paper defines a new data class called dynamic sensor network (DSN) data, for efficiently storing sensor measurements from a very dense spatial grid (very many sensing nodes). Three exact mathematical models are developed to relate observed DSN data to the underlying structural system. Candidate models are compared from a computational perspective and a truncated physical model (TPM) is presented as an efficient technique to process DSN data while reducing the size of the state variable. The role of basis functions in the approximation of mode shape regression is also established. Two examples are provided to demonstrate new applications of DSN that would otherwise be computationally prohibitive: high-resolution mobile sensing and BIGDATA processing. **DOI: 10.1061/(ASCE)EM.1943-7889.0001022.**

Author keywords: Dynamic sensor networks; Mobile sensors; BIGDATA; High spatial resolution.

Introduction

Structural health monitoring (SHM) endeavors began as observations of operational vibrations of long-span bridges as early as the 1930s (Carder 1937) with increasing participation through the 1960s (Vincent 1962). By the late 1970s, numerous modal identification studies (Abdel-Ghaffar 1976; McLamore et al. 1971; Rainer and Selst 1976; Trifunac 1970) had established promising results and provided the motivation for modern techniques. Through recent advancements in data processing, storage, mobile computing, and sensing technology, SHM techniques have evolved into repeatable, sophisticated analyses, often embedding statistical frameworks or using statistical tests for decision making (Andersen et al. 1999; Dorvash et al. 2014b; Juang and Pappa 1984; Lei et al. 2003; Shahidi et al. 2015; Smyth et al. 2003). A glimpse of the recent growth in system identification methods is particularly evident through the comparison of Abdel-Ghaffar and Scanlan (1985) and Pakzad and Fenves (2009)—two analyses of ambient vibrations observed at the Golden Gate Bridge, separated by two decades.

However, all past SHM efforts have had one common attribute: a reliance on fixed sensor networks during data collection and processing. This dependency restricts the spatial information within the observed data. For example, in system identification (SID), the spatial resolution of the mode shapes is dependent on the arrangement of the fixed sensors (Matarazzo and Pakzad 2015b). Despite numerous implementations of spatially dense sensor networks (Dorvash et al. 2014a; Inaudi and Glisic 2010; Pakzad et al. 2008; Shahidi et al. 2015; Zhu et al. 2012) once instrumented, each sensor has remained at its position throughout collection of a single data set.

In the context of this paper, a single data set is defined as a time series matrix of measured values to be processed simultaneously. Some studies have, in fact, recorded data with moving sensors; however, in such cases, either the data were split into several smaller data sets based on each sensor configuration and analyzed as fixed network data (Zhu et al. 2012) or spatial information (precise positions of the sensors) was either not measured or ignored (Cerda et al. 2012; Gonzalez et al. 2012; Lin and Yang 2005; McGetrick et al. 2009; Yang et al. 2004). Note in absence of the sensors' spatial information, the data set is not compatible with state-space approaches and a comprehensive system identification is not possible.

Moreover, for the exception of Matarazzo and Pakzad (2014, 2015b), SHM processing is currently limited to analyzing one fixed sensor network configuration at a time. Data from multiple sensor configurations must be split into multiple data sets and analyzed separately as in Zhu et al. (2012). To be clear, this is not intended to be a criticism on the direction of SHM; this is simply an exploration into a new frontier of sensing and data processing.

[1]Dept. of Civil and Environmental Engineering, Lehigh Univ., 117 ATLSS Dr., PA 18015 (corresponding author). E-mail: thomasjmatarazzo@gmail.com

[2]Associate Professor, Dept. of Civil and Environmental Engineering, Lehigh Univ., 117 ATLSS Dr., PA 18015. E-mail: pakzad@lehigh.edu

Note. This manuscript was submitted on May 14, 2015; approved on September 9, 2015No Epub Date. Discussion period open until 0, 0; separate discussions must be submitted for individual papers. This paper is part of the ***Journal of Engineering Mechanics***, © ASCE, ISSN 0733-9399.

The development and implementation of new sensor technologies as well as the techniques for processing new forms of data sets efficiently are motivated by both an improvement in extractable structural information and a reduction in network setup efforts. Subsequent new data classes often have inherently different properties in comparison to typical fixed sensor data, which dominate SHM today, and create unique processing challenges, e.g., fusion of data sampled at different rates (Smyth and Wu 2007), data with missing observations or data from mobile sensors networks (Matarazzo and Pakzad 2015b; Matarazzo et al. 2015b), or prohibitively large data dimensions of BIGDATA (Matarazzo et al. 2015a).

This paper proposes and examines dynamic sensor network data. In brief, data from a dynamic sensor network (DSN) are an amalgamation of measurements from numerous sensing configurations. The merit of DSN data is its high capacity for storing spatial information; measurements from a very large quantity of sensing nodes can be condensed into a much smaller matrix. For example, high-resolution mobile sensor networks or BIGDATA are efficiently represented in DSN data.

This paper is organized as follows. The section "Dynamic Sensor Network Data" defines fundamental properties of DSN and corresponding DSN data sets. The section "Exact State-Space Models for Dynamic Sensor Networks" presents two state-space models that have been suited for processing DSN data and introduces the truncated physical model (TPM) as an efficient model for processing data of this class. The section "Mode Shape Regression Using Basis Functions" discusses the use of the *sinc* and *spline* basis functions for approximating the *mode shape regression* term, which is included in the state-space models considered. The section "Processing Data from Novel Sensing Techniques" utilizes the proposed TPM for two novel sensing techniques: high-resolution mobile sensing and BIGDATA. Finally, the challenges in processing DSN data are summarized, the advantages of the TPM are reviewed, and a catalog of the nomenclature used among the state-space models is provided.

Dynamic Sensor Network Data

This section introduces the concept of a dynamic sensor network (DSN) and the form of its corresponding DSN data. The dynamic nature of DSN is well exemplified by a network of sensors that physically move in space while recording data in time. In this case, each sensor channel is a time series from various points in space, and when concatenated, the sensor channels form a DSN data matrix. It is fundamental that the coordinates of each sensor are known for every sample. Assume sensor locations are stored in a sensor-position matrix. Through use of this sensor-position matrix, the DSN data entries, which are mixed space-time measurements, can be decoded and properly included in a mathematical model.

Spatial discontinuities are the definitive characteristic of DSN data and are evident by inspection of the sensor-position matrix. In this case, sensing locations vary with time due to sensor mobility, and in general, a time step in which the position of any sensor changes indicates a spatial discontinuity in the DSN data matrix. This paper focuses on analyzing DSN data in this form, i.e., as a single matrix, without splitting the data into configuration-based pieces at spatial discontinuities. The remainder of this section further defines properties of DSN, DSN data, and their applications. In the following section, modeling approaches are proposed to account for the spatial discontinuities present in DSN data.

Sensors, Sensing Nodes, and Observations

In fixed sensor networks, sensing nodes are exactly the points where the sensors are installed. Typically, when these measurements are incorporated into the state-space model, the system states (structural DOF) are, by default, assigned at these same sensing nodes. In DSN, sensing nodes define the measurement space: the spatial grid that contains the recorded sensor data. Therefore, in DSN it is necessary to differentiate between these entities. For a given DSN data matrix, let the observations be the total number of columns N_O in the matrix, let the total number of sensing nodes be N, and let the total number of sensors (measurement channels) be N_{mc}. The ratios between these entities vary with each sensing technique, but in general, N is a very large integer.

General Types of DSN

A physical DSN system is not required to obtain DSN data. There are three general types of DSN data, each characterized by the source of the inherent spatial discontinuities: online, offline, and hybrid. Online DSN data come from a physical DSN, a time-varying sensor arrangement that records data, without pause, using multiple sensing configurations (groups). In this case, switches between groups are due to the physical movement of some (if not all) sensors during data collection. Offline DSN data are extracted from a fixed sensor network after data collection. For offline DSN, nearly all data parameters, including sensor group sizes and group switching schedules, are customized by the user after data collection. Lastly, hybrid DSN data combine online and offline DSN; sensing subgroups are extracted from a physical DSN, but after data collection. The following two subsections consider an application of online and offline DSN, respectively.

High-Resolution Mobile Sensing as an Online DSN

In high-resolution mobile sensing, relatively few moving sensors scan a very large number of sensing nodes. A general illustration of this form of online DSN is provided in Fig. 1, where a group of three moving sensors collects $N-2$ samples over N sensing nodes. The sensing group moves at a constant velocity and shifts to a new set of nodes after each sample, more specifically, each sensor moves to the next node to the right. The constant physical observation switching of this sampling mechanism causes spatial discontinuities in the DSN data matrix at every time step. Data collection

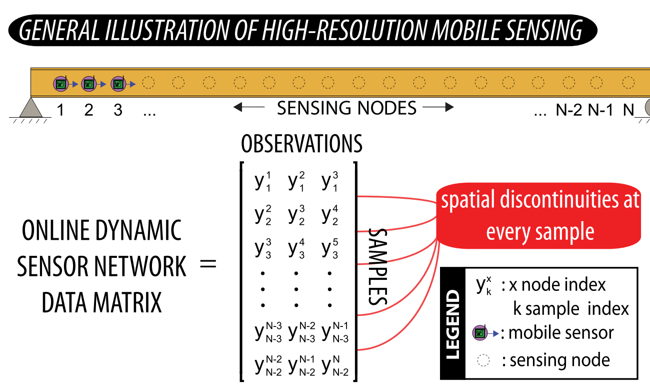

Fig. 1. General illustration of processing high-resolution mobile sensor data; three moving sensors simultaneously pass through N sensing nodes while sampling; the sensors move rightward in increments of one node per sample with $N-2$ samples in total; the corresponding online DSN data matrix is provided with spatial discontinuities at every sample F1:1

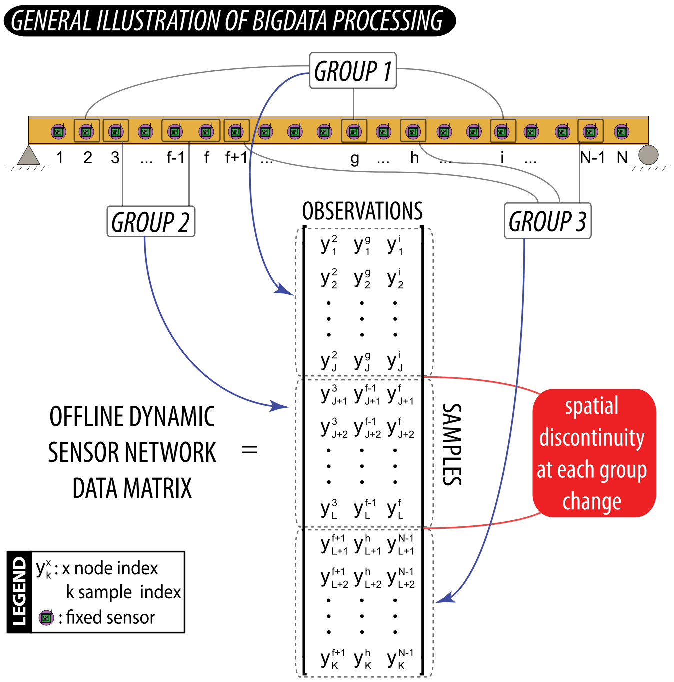

Fig. 2. General illustration of processing BIGDATA using three observations and three sensing groups: group 1 consists of nodes 2, g, and i; group 2 consists of nodes 3, $f-1$, and f; group 3 consists of nodes $f+1$, h, and $N-1$; the corresponding offline DSN data with K total samples contains two spatial continuities, one at $k = J+1$ and another at $k = L+1$

begins when all sensors are at sensing nodes on the left and ends when all sensing nodes have been scanned, i.e., $N-2$ samples in total. In this case, the observation size N_O is equal to the number of sensors N_{mc}, both of which are much smaller than the number of sensing nodes N, i.e., $N_O = N_{mc}$ and $N_O, N_{mc} \ll N$.

Processing BIGDATA as Offline DSN Data

In one definition, BIGDATA refers to a *very large* data matrix containing samples from a very large number of sensors (equally many sensing nodes), the result of a large-scale SHM endeavor. It is not feasible nor in many cases is it necessary to process all of this BIGDATA simultaneously, if at all; even simple operations such as uploading all measured data for processing could require significant computational efforts (Matarazzo et al. 2015a). A useful strategy is to extract an information-packed subset, an offline DSN data set, from the BIGDATA population, i.e., a user-selected data matrix in which a vast amount of spatial information is condensed into a small size. A benefit of this approach is the high versatility of offline DSN data. Given BIGDATA, there are numerous potential offline DSN data sets since the user has the ability to choose every entry of the subset, which can be of any size (of course, not exceeding BIGDATA dimensions).

A general illustration of this type of offline DSN data is provided in the example in Fig. 2 where three distinct sensing groups form the data matrix: group 1 includes nodes 2, g, and i; group 2 includes nodes 3, $f-1$, and f; group 3 includes nodes $f+1$, h, and $N-1$. The $K \times N_O$ DSN data matrix contains spatial discontinuities at $k = J+1$ and $k = L+1$ corresponding with user-selected sensing groups. In this case, the observation size is three ($N_O = 3$), which is much smaller than the number of fixed sensors instrumented at the sensing nodes, i.e., $N_O \ll N_{mc}$ and $N_{mc} = N$.

Exact State-Space Models for Dynamic Sensor Networks

This section introduces exact state-space models in which underlying state DOF responses are mapped from DSN data. The following subsections present three state-space models that represent a structural system exactly and have been tailored to incorporate DSN data properly. The sizes of these models and their corresponding efficiencies are discussed and compared. The first two subsections present modified versions of the familiar standard and modal state-space models that simultaneously consider a small number of observations (N_O data columns) and a large number of sensing nodes (N locations); in these situations, the benefits of DSN data are most evident. The adjustments to these models have a physical significance: they relate the structural response at one location to the response at another. Despite their similar mathematical forms, each model has distinct attributes and challenges.

In the third subsection, the truncated physical model (TPM) is introduced as an efficient solution for modeling DSN observations. In this context, an efficient model remains exact and requires minimal computational efforts; this is dictated by the sizes of model parameters (matrices), which are dependent on the definitions of the state variable and the observations.

Consider the second-order continuous-time equation of motion for a linear N-DOF system, where N is a very large integer

$$\bar{m}\,\ddot{\mathbf{u}}(t) + \bar{c}\,\dot{\mathbf{u}}(t) + \bar{k}\mathbf{u}(t) = B_f\boldsymbol{\eta}(t) \tag{1}$$

The locations of the N lumped masses are defined by the spatial vector $\mathbf{s} = [s_1 \quad s_2 \quad \dots \quad s_N]^T$. Note there is a DOF at every sensing node, i.e., they are coincident. Sampled structural responses (at sampling rate $f_s = 1/\Delta t$) are available at all DOF via the full spatial vector $\mathbf{s}$. Similarly, a general subset of these DOF, called $\mathbf{s}_i$, is comprised of some elements in $\mathbf{s}$, i.e., $\mathbf{s}_i \subset \mathbf{s}$, and refers to responses at selected DOF. Various spatial subvectors of this form will be introduced to reference specific DOF subsets, as opposed to all N DOF at once. The structural responses considered are defined for time steps $k = 1, 2, \dots, K$: where $\mathbf{u}_k(\mathbf{s}_i)$ is a vector of displacements at DOF defined by $\mathbf{s}_i$ at time step k; $\dot{\mathbf{u}}_k(\mathbf{s}_i)$ is a vector of velocities at DOF defined by $\mathbf{s}_i$ at time step k; and $\ddot{\mathbf{u}}_k(\mathbf{s}_i)$ is a vector of accelerations at DOF defined by $\mathbf{s}_i$ at time step k.

In this section, the standard state-space model, modal state-space model, and truncated physical model (TPM) are formulated with the objective of using field measurements (observations) at N_O sensing nodes defined by $\mathbf{s}_O \subset \mathbf{s}$ to describe the behavior of the structural system through the state variable, e.g., $\mathbf{x}_k$. The observation vector $\mathbf{y}_k$ describes the exact responses at N_O DOF defined by $\mathbf{s}_O \subset \mathbf{s}$ as shown in Eq. (2) and remains valid for all subsequent state-space models

$$\mathbf{y}_k \equiv \ddot{\mathbf{u}}_k(\mathbf{s}_O) \tag{2}$$

Some final notes are necessary before the models are presented. The primary difference between typical state-space models for fixed sensor networks and those for dynamic sensor networks (DSN) (which are presented in the following subsections) is that the latter require the sensors' positions to be known precisely. For DSN, the locations of the observations will be a function of time step k, i.e., $O = O(k)$. Consider $\mathbf{s}_O$ as the kth row (transposed) of a $K \times N_O$ sensor-position matrix, S_O, corresponding to the sensors in the DSN data matrix. For simplicity, this will not be explicitly included in successive notation; however, in the following subsections, model entities that depend on $\mathbf{s}_O$ will also vary at every time step, e.g., Φ_O.

Nomenclature tables are provided at the end of the paper for reference to model entities. Lastly, theoretically, the model orders for each subsequent state-space model, p, are all equal to 2; however, since significantly higher model orders are commonly considered in system identification applications (Chang and Pakzad 2013), a general definition is presented when referring to vector and matrix sizes.

Standard State-Space Model

This subsection presents the first state-space model under consideration for DSN: the standard state-space model. In this framework, the state vector $\mathbf{x}_k$, shown in Eq. (3), represents structural responses at all N DOF as defined by $\mathbf{s}$

$$\mathbf{x}_k \equiv \begin{bmatrix} \mathbf{u}_k(\mathbf{s}) \\ \dot{\mathbf{u}}_k(\mathbf{s}) \end{bmatrix} \tag{3}$$

Also, given the full mode shape matrix $\Phi = \Phi^{\langle M\rangle}(\mathbf{s})$, where Φ is an $N \times M$ matrix (inherently truncated to $M = N$ modes due to mass discretization), submode shapes matrices $\Phi_i = \Phi^{\langle M\rangle}(\mathbf{s}_i)$ describe modal ordinates for respective spatial subvectors, e.g., $\Phi_O = \Phi^{\langle M\rangle}(\mathbf{s}_O)$ is an $N_O \times M$ matrix. Eqs. (4) through (8) provide discrete-time state-space model parameters

$$A_c \equiv \begin{bmatrix} 0 & I \\ -\bar{m}^{-1}\bar{k} & -\bar{m}^{-1}\bar{c} \end{bmatrix} \tag{4}$$

$$A = \exp(A_c \Delta t) \tag{5}$$

$$B_c \equiv \begin{bmatrix} 0 \\ -\bar{m}^{-1}B_f \end{bmatrix} \tag{6}$$

$$B = A_c^{-1}(A - I)B_c \tag{7}$$

$$C \equiv C_a[-\bar{m}^{-1}\bar{k} \quad -\bar{m}^{-1}\bar{c}] \tag{8}$$

Once the parameters are defined, the second-order differential equation is expressed in first-order form through the state Eq. (9) and the observation Eq. (10) for DSN

$$\mathbf{x}_k = A\mathbf{x}_{k-1} + B\boldsymbol{\eta}_{k-1} \tag{9}$$

$$\mathbf{y}_k = \Phi_O\Phi^{-1}C\mathbf{x}_k \tag{10}$$

Along the usual model parameters (Juang and Phan 2001), the product $\Phi_O\Phi^{-1}$ is added to the observation equation. This term represents the regression of the responses at $\mathbf{s}$ on those at $\mathbf{s}_O$ and is the key to modeling the dynamics of one set of DOF while observing another; this entity is henceforth called the *mode shape regression* (MSR) term. More specifically, the acceleration responses $\ddot{\mathbf{u}}_k(\mathbf{s}) = C\mathbf{x}_k$ are first converted to modal coordinates through Φ^{-1}, then reverted to physical coordinates using Φ_O, finally representing $\mathbf{y}_k = \ddot{\mathbf{u}}_k(\mathbf{s}_O)$, in other words, $\ddot{\mathbf{u}}_k(\mathbf{s}_O) = \Phi_O\Phi^{-1}\ddot{\mathbf{u}}_k(\mathbf{s})$. In the case that all DOF are observed, $\mathbf{s}_O = \mathbf{s}$, $\Phi_O\Phi^{-1} = I$, and the familiar observation equation $\mathbf{y}_k = C\mathbf{x}_k$ is obtained.

In review of the standard model, the state variable represents all N DOF and the observations measure responses at N_O DOF. Thus, $\mathbf{y}_k$ is an $N_O \times 1$ vector, $\mathbf{x}_k$ is a $pN \times 1$ vector, the state matrix A is $pN \times pN$, the observation matrix C is $N_O \times pN$, and the mode shape regression matrix $\Phi_O\Phi^{-1}$ is $N_O \times N$ (recall $M = N$).

However, this model is unmanageably large when N is very large and thus is unsuitable for DSN. In this framework, the number of DOF (state variables) is coupled with the sensing nodes; they are coincident. In other words, a high spatial resolution requires an overly complex dynamic model. Furthermore, the state variable size is very large (too large for system identification methods as one of the users of such models). For common networks, the required computational efforts for model-order-selection-based structural modal identification of fixed sensing networks are substantial (Chang and Pakzad 2012; Pakzad and Fenves 2009) and greatly sensitive to the size of the state variable (Matarazzo et al. 2015a). For a very large N, this model is impractical for modal identification purposes. In consideration of an efficient model for DSN, it is illogical for all sensing nodes and states to coincide as required by this model; it is thus desirable to implement a model capable of distinguishing between these entities.

Modal State-Space Model

This subsection presents the second state-space model under consideration for DSN: the modal state-space model. In this approach, the observations represent the same entities as before, i.e., $\mathbf{y}_k = \ddot{\mathbf{u}}_k(\mathbf{s}_O)$; however, the states, provided by Eq. (11), represent modal responses

$$\mathbf{z}_k \equiv [\, \mathrm{q}_k^{\langle 1\rangle} \quad \dots \quad \mathrm{q}_k^{\langle M\rangle} \quad \dot{\mathrm{q}}_k^{\langle 1\rangle} \quad \dots \quad \dot{\mathrm{q}}_k^{\langle M\rangle} \,]^T \tag{11}$$

The sampled modal responses are defined for all time steps $k = 1, 2, \dots, K$ and all modes $m = 1, 2, \dots, M$, where $\mathrm{q}_k^{\langle m\rangle}$ is the sampled modal displacement for mode m at time step k; $\dot{\mathrm{q}}_k^{\langle m\rangle}$ is the sampled modal velocity for mode m at time step k; and $\ddot{\mathrm{q}}_k^{\langle m\rangle}$ is the sampled modal acceleration for mode m at time step k.

Along this new state variable, the remaining state terms are defined for modal space using M modal equations of motion (see Chapter 12 of Chopra 2007 for details). The modal mass matrix, modal stiffness matrix, modal damping matrix, and modal inputs in Eqs. (12) through (15) are found using modal superposition and the modal equations of motion

$$\bar{M} \equiv \Phi^T\bar{m}\Phi \tag{12}$$

$$\bar{K} \equiv \Phi^T\bar{k}\Phi \tag{13}$$

$$\bar{C} \equiv \Phi^T\bar{c}\Phi \tag{14}$$

$$\boldsymbol{\upsilon}_k \equiv \Phi^T\boldsymbol{\eta}_k \tag{15}$$

The full mode shape matrix and the submode shape matrix are identical to those in the standard state-space model: $\Phi = \Phi^{\langle M\rangle}(\mathbf{s})$ is an $N \times M$ matrix and $\Phi_O = \Phi^{\langle M\rangle}(\mathbf{s}_O)$ is an $N_O \times M$ matrix. The modal state-space model parameters provided in Eqs. (16) through (20) are analogous to the physical model counterparts from Eqs. (4) through (8)

$$A_c^{\langle M\rangle} \equiv \begin{bmatrix} 0 & I \\ -\bar{M}^{-1}\bar{K} & -\bar{M}^{-1}\bar{C} \end{bmatrix} \tag{16}$$

$$A^{\langle M\rangle} = \exp(A_c^{\langle M\rangle}\Delta t) \tag{17}$$

$$B_c^{\langle M\rangle} \equiv \begin{bmatrix} 0 \\ -\bar{M}^{-1}B_f \end{bmatrix} \tag{18}$$

$$B^{\langle M\rangle} = (A_c^{\langle M\rangle})^{-1}(A^{\langle M\rangle} - I)B_c^{\langle M\rangle} \tag{19}$$

$$C^{\langle M\rangle} \equiv C_a^{\langle M\rangle}[\,-\bar{M}^{-1}\bar{K} \quad -\bar{M}^{-1}\bar{C}\,] \tag{20}$$

Finally, note $\mathrm{p}_k^{\langle m\rangle}$ is the sampled modal input for mode m at time step k

$$\boldsymbol{\upsilon}_k \equiv [\,\mathrm{p}_k^{\langle 1\rangle} \quad \ldots \quad \mathrm{p}_k^{\langle M\rangle}\,]^T \tag{21}$$

The M second-order differential equations representing the modal equations of motion are expressed in first-order form through the modal state Eq. (22) and a physical-modal observation Eq. (23) for DSN

$$\mathbf{z}_k = A^{\langle M\rangle}\mathbf{z}_{k-1} + B^{\langle M\rangle}\boldsymbol{\upsilon}_{k-1} \tag{22}$$

$$\mathbf{y}_k = \Phi_O C^{\langle M\rangle}\mathbf{z}_k \tag{23}$$

The wording physical-modal is intended to acknowledge that observations and states are in different coordinate systems, physical and modal, respectively. In this model, the observation matrix represents modal coordinates; thus, mode shape regression, i.e., premultiplication by Φ^{-1}, is no longer necessary. In Eq. (23), modal state responses are mapped to physical measurements through the modal observation matrix $C^{\langle M\rangle}$ and observation submode shape matrix Φ_O. With this framework, the observation subvector $\mathbf{s}_O$ and corresponding submode shape matrix Φ_O account for variations in sensor configurations; all other model parameters are preserved.

In review of the modal model, the state variable represents all M modal responses and the observations measure physical responses at N_O DOF. Thus, $\mathbf{y}_k$ is an $N_O \times 1$ vector, $\mathbf{z}_k$ is a $pM \times 1$ vector, the state matrix $A^{\langle M\rangle}$ is $pM \times pM$, the observation matrix $C^{\langle M\rangle}$ is $M \times pM$, and the submode shape matrix for the observations Φ_O is $N_O \times M$. Now if $M = N$, the model parameters are as large as before, in which case, the modal model offers no evident improvement over the standard model. However, the number of sensing nodes is no longer coupled with the state variable; thus, one issue with the previous model has been resolved. Furthermore, if the modes are truncated so that M is considerably smaller than N, for example, $M = N_O$ (note $N_O \leq M \leq N$), then, the advantages of this model become quite apparent. The number of modal responses included dictates the size of this modal model, whereas the size of the standard model is defined by the total number of sensing nodes. Moreover, the practice of modal truncation, i.e., the selection of M, is a familiar decision in structural dynamics for systems with large DOF and the assumption leads clear theoretical consequences [see section 19.7 in Chopra (2007)].

With the state variable decoupled from the model DOF, the state size is independent of the total number of sensing nodes and the model complexity is reduced from pN in the standard model to pM in this modal model. There are three main benefits of this reduction: a significantly smaller model, model complexity is user selected through M, and the significance of this selection is intuitive as it is equivalent to modal truncation.

In conclusion, the modal state-space model is an attractive choice for modeling structural systems using DSN data. However, the model contains the following two pitfalls:

1. The states represent modal responses, while the observations are in physical coordinates. In system identification, it is counterintuitive to decompose the measured signal into modal components without knowledge of the modal properties of the structural system, i.e., prior to identification. Moreover, assuming $\mathbf{z}_k$, $A^{\langle M\rangle}$, and $C^{\langle M\rangle}$ are available, a coordinate transformation would be required to extract corresponding spatial information in the physical space. In short, with a modal state variable, physical mode shapes are not available directly after model identification.
2. The submode shape matrix for the observations Φ_O is a function of the time step since the locations of the observations $\mathbf{s}_O$ vary over time, i.e., $O = O(k)$. This feature yields a linear parameter varying (LPV) state-space model, complicating system identification procedures.

The following subsection presents a truncated physical model (TPM), which maintains the benefits of the modal state-space model and addresses the aforementioned challenges.

Truncated Physical Model

Previous state-space approaches in this paper have adapted existing models to include DSN data as observations, primarily mapping states to measured values using the submode shape for the observations. This section presents a novel state-space technique for DSN data: the truncated physical model (TPM). The TPM assumes the modal state-space model (from the previous section) was the result of a coordinate transformation T, which mapped modal states $\mathbf{z}$ to truncated physical states $\mathbf{x}^*$ via $\mathbf{x}^* = T\mathbf{z}$. Motivated from the challenges of implementing the modal state-space model for DSN, the goal of the TPM is to transform the modal matrices so that the state variable represents responses in physical (not modal) coordinates. It will be shown that, after this transformation, a truncated modal space yields a reduced (truncated) physical space for the states while the sensing nodes are unaffected. The benefits of modal truncation are mapped into a reduced, but not restricted, physical state representation of the dynamic system. The assumed transformation exclusively activates N_α user-selected DOF, specified by $\mathbf{s}_\alpha \subset \mathbf{s}$ and $\mathbf{s}_\alpha \neq \mathbf{s}$ (otherwise, the benefits of this transformation are lost), with $\Phi_\alpha = \Phi^{\langle M\rangle}(\mathbf{s}_\alpha)$, where Φ_α is an $N_\alpha \times M$ matrix. The locations specified by $\mathbf{s}_\alpha$ are hereafter named *virtual probing locations* (VPL). It will be shown that the states are the responses at these VPL.

For simplicity and minimum model size, it is assumed that the number of observations in the DSN data matrix, the number of modal responses included in the dynamic system, and the number of VPL are all equal, i.e., $N_O = M = N_\alpha$; note the minimum value for M is selected. The $pN_\alpha \times pM$ transformation matrix T is defined in Eq. (24) with square, block diagonal entries Φ_α

$$T \equiv \begin{bmatrix} \Phi_\alpha & 0 \\ 0 & \Phi_\alpha \end{bmatrix} \tag{24}$$

The transformation matrix relates TPM parameters (denoted by superscript *) to modal model parameters [denoted by superscript $\langle M\rangle$]

$$A^{\langle M\rangle} \equiv T^{-1}A^*T \tag{25}$$

$$B^{\langle M\rangle} \equiv T^{-1}B^* \tag{26}$$

$$C^{\langle M\rangle} \equiv C^*T \tag{27}$$

The preceding equations are rearranged (*back-transformed*) to define TPM parameters in terms of modal model parameters

$$A^* = TA^{\langle M\rangle}T^{-1} \tag{28}$$

$$B^* = TB^{\langle M\rangle} \tag{29}$$

$$C^* = C^{\langle M\rangle}T^{-1} \tag{30}$$

The back-transformation results in physical responses at $\mathbf{s}_\alpha$, while the observations are unaltered. In other words, unlike the modal model, the TPM is exclusively defined in physical coordinates. Note $\mathbf{s}_\alpha \neq \mathbf{s}$ and $\mathbf{s}_\alpha$ contains significantly fewer elements than $\mathbf{s}$, i.e., $N_\alpha \ll N$; otherwise, the benefits of this back-transformation would be lost. The $pN_\alpha \times 1$ TPM state vector is defined by the spatial vector $\mathbf{s}_\alpha$; therefore, the responses at the VPL dictate the dynamic model

$$\mathbf{x}_k^* \equiv \begin{bmatrix} \mathbf{u}_k(\mathbf{s}_\alpha) \\ \dot{\mathbf{u}}_k(\mathbf{s}_\alpha) \end{bmatrix} \tag{31}$$

It is important to reiterate that this reduction in physical space is not restrictive. In other words, the VPL can represent any user-selected DOF subset defined by $\mathbf{s}_\alpha \subset \mathbf{s}$ and T accordingly, a trait unique to the TPM

$$\mathbf{x}_k^* = A^* \mathbf{x}_{k-1}^* + B^* \mathbf{\upsilon}_{k-1} \tag{32}$$

$$\mathbf{y}_k = \Omega \Phi_\alpha C^* \mathbf{x}_k^* \tag{33}$$

In Eq. (34), an MSR term is represented by Ω, an $N_O \times M$ matrix

$$\Omega \equiv \Phi_O \Phi_\alpha^{-1} \tag{34}$$

Similar to the MSR term found in Eq. (11) for the standard state-space model, the term in Eq. (34) represents the regression of the ordinates at the VPL responses (defined by $\mathbf{s}_\alpha$) on to those at the observations (defined by $\mathbf{s}_O$). In other words, $\Omega = \Phi_O \Phi_\alpha^{-1}$ maps the VPL responses $\ddot{\mathbf{u}}_k(\mathbf{s}_\alpha) = \Phi_\alpha C^* \mathbf{x}_k^*$ to the observations $\ddot{\mathbf{u}}_k(\mathbf{s}_O)$, i.e., $\ddot{\mathbf{u}}_k(\mathbf{s}_O) = \Psi \ddot{\mathbf{u}}_k(\mathbf{s}_\alpha)$. Unlike the modal model, the TPM has a physical state variable, so that when the state matrix and the observation matrix are available, the corresponding mode shapes cover VPL nodes. For example, in system identification, physical mode shapes can be computed directly from these model parameters: the eigendecomposition of A^* yields natural frequencies and damping ratios, and $\Phi_\alpha C^*$ provides submode shapes at VPL.

In review of the TPM, the size and locations (VPL) of the truncated physical states are user defined, through N_α and $\mathbf{s}_\alpha$, respectively. Also, truncated physical states are exact truncated physical responses at the VPL. In general, the observation vector $\mathbf{y}_k$ is $N_O \times 1$, the truncated physical state vector $\mathbf{x}_k^*$ is $pN_\alpha \times 1$, the truncated physical state matrix A^* is $pN_\alpha \times pN_\alpha$, the truncated physical observation matrix C^* is $M \times pN_\alpha$, the submode shape term for VPL Φ_α is $N_\alpha \times M$, and the MSR term Ω is $N_O \times M$. With the assumption for minimum model size $N_\alpha = N_O = M$, the model complexity is reduced significantly and becomes directly related to the number of observations in the DSN data matrix. More specifically, $\mathbf{x}_k^*$ is $pN_O \times 1$, A^* is $pN_O \times pN_O$, C^* is $N_O \times pN_O$, Φ_α is $N_O \times N_O$, and Ω is $N_O \times N_O$.

In conclusion, the TPM establishes an intuitive relationship between the observation size of the DSN data matrix and the complexity of the underlying dynamic states. More importantly, model complexity and state DOF are independent of the full set of sensing nodes. This is a vast improvement on the coupled nature between states and sensing nodes observed in the standard state-space model. Additionally, with physical, user-defined VPL states, the interpretation of identified modal properties is simplified.

As with other state-space models (Matarazzo and Pakzad 2015a; Matarazzo et al. 2015a; Peeters and De Roeck 1999), an additive noise term can be included in the observation equation of the TPM. Eq. (33) can be modified to $\mathbf{y}_k = \Omega \Phi_\alpha C^* \mathbf{x}_k^* + \mathbf{w}_k$, to properly, and simply, include sensor noise $\mathbf{w}_k$, which is independent of the true structural response. There are no particular restrictions on sampling frequency required by the TPM or DSN data other than consideration of the Nyquist frequency (Oppenheim et al. 1999) to prevent temporal aliasing.

It is important to mention that Ω is a time-variant parameter because it is a function of Φ_O. The merit of Ω is that it can be approximated efficiently by a basis function for spatial reconstruction, without knowledge of the true structural mode shapes. With this approximation, the challenges of system identification of a LPV state-space model (as mentioned at the end of the previous section) can be eliminated. This topic is further discussed in the following section.

Mode Shape Regression Using Basis Functions

In this section, the role of basis functions for the use in the TPM is discussed. It is shown that the MSR term Ω [introduced in Eq. (34)] can be approximated by the use of basis functions. Furthermore, accurate estimates of DSN data in time and frequency domain become available in the TPM through a simple technique, without additional use of true structural mode shapes. Moheimani et al. (2003) presented linear reconstruction of structural mode shapes using Shannon sampling theorem for discrete signals, henceforth WKS (Whitaker, Kotelnikov, Shannon) theory. Portions of this theorem and its extensions can be attributed to Whittaker (1915, 1928), Kotelnikov (1933), or Shannon (1998); in this paper, the term WKS is adopted from Jerri (1977), which refers to the authors' collective contributions. The application of WKS is revisited using nomenclature familiar to the previous section; then, the relation is adapted for use in the truncated physical state-space model.

The approach begins with an ideal, regular sampling case: first assume sensing nodes are defined by $\mathbf{s} = [s_1 \quad s_2 \quad \dots \quad s_N]^T$. Eq. (35) below reformulates Eq. 7.39 from Moheimani et al. (2003) for approximation of the $N \times M$ full mode shape $\Phi = \Phi^{\langle M \rangle}(\mathbf{s})$ using an $N_\chi \times M$ subset mode shape $\Phi_\chi = \Phi^{\langle M \rangle}(\mathbf{s}_\chi)$, where $\mathbf{s}_\chi = [s_{\chi_1} \quad s_{\chi_2} \quad \dots \quad s_{\chi_\beta}]^T$ is uniformly spaced on the structure at Δs_χ and $\mathbf{s}_\chi \subset \mathbf{s}$

$$\hat{\Phi} = \left[\operatorname{sinc}\left(\frac{1}{\Delta s_\chi}(\mathbf{s} - s_{\chi_1})\right) \quad \operatorname{sinc}\left(\frac{1}{\Delta s_\chi}(\mathbf{s} - s_{\chi_2})\right) \quad \dots \quad \operatorname{sinc}\left(\frac{1}{\Delta s_\chi}(\mathbf{s} - s_{N_\chi})\right) \right] \Phi_\chi \tag{35}$$

Note the estimate $\hat{\Phi}$ is an $N \times M$ matrix, which is exact at N_χ subset locations, i.e., $\hat{\Phi}(\mathbf{s}_\chi) = \Phi(\mathbf{s}_\chi) = \Phi_\chi$, because $\operatorname{sinc}(0) = 1$. Mode shape ordinate approximations at remaining $N - N_\chi$ locations, i.e., $\hat{\Phi}(\mathbf{s} \not\subset \mathbf{s}_\chi)$, are interpolated through this reconstruction. As in the case with temporal sampling, it is essential to anticipate the highest expected frequency content of the wave when selecting a spatial sampling frequency. In the case of a simply supported beam with N uniformly spaced nodes and length L, in order to avoid spatial aliasing, sensing nodes must be spaced so that $\Delta s_\chi < L/N$. Additional details on the reconstruction accuracy and its corresponding error at sensing nodes, namely $\varepsilon \equiv \|\hat{\Phi} - \Phi\|_2$, can be found in reconstruction literature (Moheimani et al. 2003;

Jagerman and Fogel 1956; Jerri 1977; Stenger 1976; Whittaker 1915).

The next step will focus on the interpolated portions of the mode shape estimates. Two subsets of sensing nodes and their corresponding submode shapes will be defined, and then related using the same aforementioned theory. Finally, the relation between the submode shapes will be rearranged, to prove that the *sinc* basis function approximates the MSR term in the TPM.

Consider WKS for the problem of estimating modal ordinates at a different subset mode shape matrix, say Φ_δ, using Φ_χ. In other words, define a different subset of modal ordinates $\Phi_\delta = \Phi^{\langle M\rangle}(\mathbf{s}_\delta)$ of equal size, i.e., $N_\delta = N_\chi$, where $\mathbf{s}_\delta = [\, s_{\delta_1} \quad s_{\delta_2} \quad \ldots \quad s_{N_\delta}\,]^T$ and $\mathbf{s}_\delta \subset \mathbf{s}$. Additionally, assume no overlapping locations between these two sensing node subsets, i.e., their union is null $\mathbf{s}_\chi \cap \mathbf{s}_\delta = \emptyset$ (this is to demonstrate maximum utility; it is not a requirement). The estimation of Φ_δ is given in Eq. (36), where the WKS reconstruction has been adjusted to exclusively represent interpolation. More specifically, the following equation defines linear regression of one set of modal ordinates onto another where the entries of the basis function matrix Ω_{sinc} are the regression coefficients

$$\hat{\Phi}_\delta = \left[\operatorname{sinc}\left(\frac{1}{\Delta s_\chi}(\mathbf{s}_\delta - s_{\chi_1})\right) \quad \operatorname{sinc}\left(\frac{1}{\Delta s_\chi}(\mathbf{s}_\delta - s_{\chi_2})\right) \quad \ldots \quad \operatorname{sinc}\left(\frac{1}{\Delta s_\chi}(\mathbf{s}_\delta - s_{N_\chi})\right)\right]\Phi_\chi$$

$$\hat{\Phi}_\delta = \Omega_{\text{sinc}}\Phi_\chi \tag{36}$$

Both sides of the equation above are postmultiplied by Φ_χ^{-1} resulting in Eq. (37)

$$\Omega_{\text{sinc}} = \hat{\Phi}_\delta\Phi_\chi^{-1} \tag{37}$$

Eq. (37) has a great significance in the context of the TPM. The left-hand side of Eq. (37) is the *sinc* basis evaluated at the lags between locations $\mathbf{s}_\delta$ and $\mathbf{s}_\chi$; the right-hand side of Eq. (37) is an approximation for the MSR term that relates $\ddot{\mathbf{u}}_k(\mathbf{s}_\delta)$ and $\ddot{\mathbf{u}}_k(\mathbf{s}_\chi)$ to each other. In other words, the *sinc* basis function approximates the MSR term. Furthermore, with $\Phi_\delta = \Phi_O$ and $\Phi_\chi = \Phi_\alpha$, through the proper selections of $\mathbf{s}_\delta$ and $\mathbf{s}_\chi$, the *sinc* basis matrix is an estimator for Ω [found in the TPM, Eq. (34)]. *Sinc* is not the only basis capable of estimating the MSR term. As discussed in Butzer et al. (1986), Moheimani et al. (2003), and Unser (1999), *B-splines* are a computationally efficient replacement for a *sinc* basis and carry useful curvature and derivative properties. The substitution in Eq. (38) provides an estimate for Ω, which is, in general, less accurate than Ω_{sinc}; however, *B-splines* provide the "best performance for the least complexity" (Unser 1999)

$$\Omega_{\text{spline}} = [\,\beta^n(\mathbf{s}_\delta - s_{\chi_1}) \quad \beta^n(\mathbf{s}_\delta - s_{\chi_2}) \quad \ldots \quad \beta^n(\mathbf{s}_\delta - s_{N_\chi})\,] \tag{38}$$

The variable complexity and performance of *B-splines* is characterized by the selection of degree n. In many applications, the cubic spline, $n = 3$, is a popular choice due to its minimum curvature property, and in fact, as the *spline* degree goes to infinity, the cardinal *spline* filter approaches the ideal *sinc* filter (Aldroubi et al. 1992).

Most importantly, the requirement of uniformly spaced sensing nodes is not necessarily a restriction since in the TPM, the VPL are arbitrary; they are chosen by the user out of all sensing nodes. Therefore, the user can simply program VPL to be uniformly spaced nodes and achieve optimal results (maximum accuracy of the MSR approximation). Also note, for irregular or nonperiodic VPL, the WKS relations presented in this section remain applicable; however, the corresponding error has a different form (Beutler 1961, 1966). It is recommended that the VPL are selected to be uniformly spaced.

Processing Data from Novel Sensing Techniques

This section presents novel sensing applications of the modal model and the truncated physical model (TPM). As discussed in previously, the TPM computes dynamic sensor network (DSN) data efficiently at a model complexity, which depends on the modal truncation—not the quantity of sensing nodes. The implementation of a minimum complexity TPM to compute DSN data is essential to the eventual practice of such sensing systems. The following applications have three primary objectives:

1. Demonstrate that the proposed TPM provides responses identical to the theory. In these studies, the theoretical solution is represented by the modal state-space model, which provides the exact structural responses truncated to M modes.
2. Quantify the accuracy of the mode shape regression (MSR) term approximations computed using *sinc* and *spline* basis functions.
3. Provide two examples of novel sensing techniques that can be modeled exactly and efficiently (at the minimum model size) using DSN data and the TPM.

In both applications, the SHM of a flexible beam structure using 5,000 sensing nodes is considered. The high-resolution mobile sensing case exemplifies online DSN data, while the BIGDATA case demonstrates offline DSN data. In each case, the spatial discontinuities in the DSN data matrix have a different source. In high-resolution sensing, the discontinuities are due to the physical movement of the sensors, while in BIGDATA, they are a result of user-selected sensor scheduling, after data collection. Moreover, the specific offline DSN application extracted from the raw data represents only a single hypothetical data set out of the voluminous possibilities available with BIGDATA.

High-Resolution Mobile Sensing Application

In this section, the response of a flexible simple beam is measured by 19 mobile sensors, which scan 5,000 sensing nodes. Four models are considered to simulate the resulting online DSN data set: modal model, TPM, TPM with *sinc* bases, and TPM with cubic *splines*. The modal and TPM are exact and theoretically equivalent, while the TPM with a basis function is approximate.

In this application, a 5,000-DOF beam is subjected to a vertical white noise ground motion at the supports with a frequency cut off at 30 Hz. The natural vibration properties of the beam are provided in Table 1, with natural frequencies ranging from 0.27 to 98.19 Hz.

Table 1. First 19 Natural Vibration Properties of 5,000-DOF Beam

Mode	Frequency (Hz)	Damping (%)
1	0.273	0.027
2	1.09	0.108
3	2.45	0.244
4	4.35	0.434
5	6.80	0.678
6	9.79	0.977
7	13.33	1.33
8	17.41	1.74
9	22.03	2.20
10	27.20	2.71
11	32.91	3.28
12	39.17	3.91
13	45.97	4.58
14	53.31	5.32
15	61.20	6.10
16	69.63	6.94
17	78.60	7.84
18	88.12	8.79
19	98.19	9.79

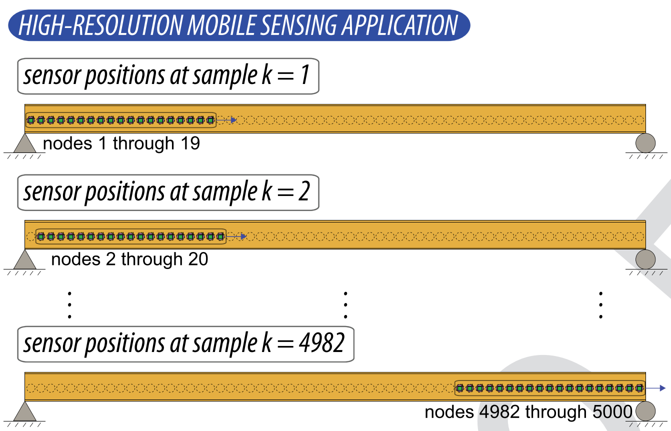

Fig. 3. Positions of mobile sensors at selected samples in high-resolution mobile sensing application; 19 sensors scan 5,000 sensing nodes as a group, shifting rightward to the next node after each sample

Fig. 3 depicts the mobile sensing network for this application, which samples at a rate of 200 Hz. The DSN is a group of 19 neighboring sensors that scan the structural response by shifting together, after each sample, in increments of one sensing node. At sample $k = 1$, the sensor group measures responses at sensing nodes 1 through 19; at sample $k = 2$, they observe sensing nodes 2 through 20; finally, at sample $k = K = 4{,}982$, they observe sensing nodes 4,982 through 5,000. The resulting online DSN data matrix is $19 \times 4{,}982$ and includes information from all 5,000 sensing nodes.

The exact modal responses are calculated for the first 19 modes ($M = 19$) using a modal state-space model. With this information, the exact truncated responses can be computed at all DOF through the use of a spatially dense mode shape vector. However, it is only necessary to compute responses at locations and times where the DSN is scheduled to cover. As presented earlier, the submode shape term is added to the modal state-space model to calculate the observations of an online DSN. The resulting DSN data are the exact truncated measurements.

Using the same loading, the TPM is constructed in accordance with its introductory section with 19 VPL selected uniformly across the beam; thus, for the minimum model size, 19 structural modes were included. The modal model computed DSN data directly from modal responses of the state variable. The TPM computes DSN data (observations) from the truncated physical states, the exact truncated physical responses at VPL DOF.

Mobile Sensing Results

In Fig. 4, the responses at mobile sensors 1, 10, and 19 are compared over a selected range of samples. The individual responses of the moving sensors are redundant as the range of sensing nodes covered by the group is quite small, covering only 0.38% of the beam at each sample. The DSN data from the modal and TPM are nearly identical, as they are theoretically equivalent; any differences are the result of computational error, predominantly, the matrix inversion required in the TPM by $\Omega = \Phi_O \Phi_\alpha^{-1}$. As expected, the computational error for the mobile sensing DSN data (over 94,000 entries) is small, with a mean squared error (MSE) equal to 16.54×10^{-5}.

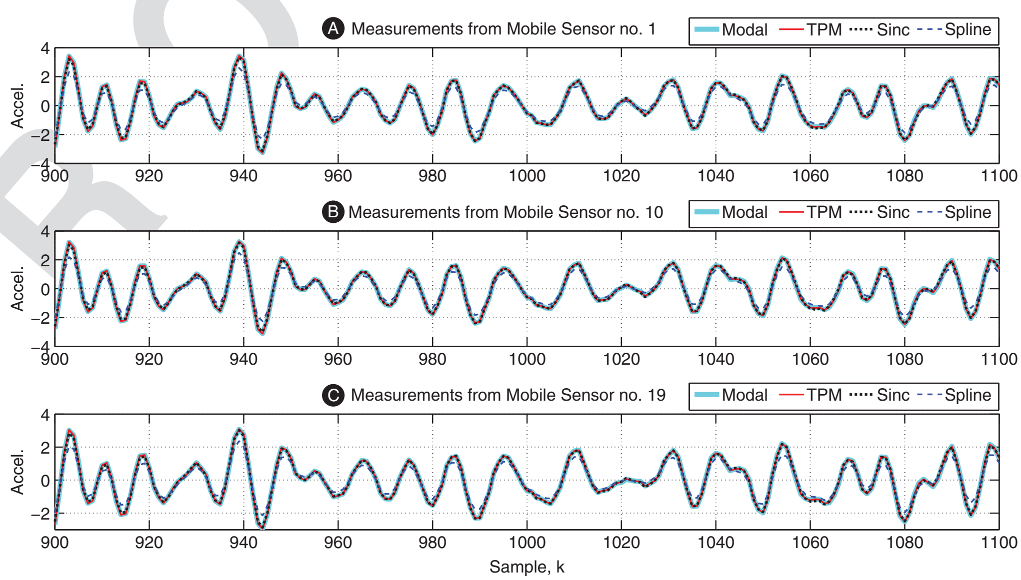

Fig. 4. Comparison of data from modal, TPM, and TPM with basis approximations for samples 900 through 1,100 for mobile: (a) sensor 1; (b) sensor 10; (c) sensor 19

Table 2. Comparison of Online DSN Data in Mobile Sensing Application

Error type	Sum of squares in time domain	Time domain MSE	Sum of squares of PSD	PSD MSE
Computational $\sum_{k,s_o}(Y_{\text{modal}} - Y_{\text{TPM}})^2$	15.66	16.54×10^{-5}	11.72×10^{-4}	60.21×10^{-9}
Sinc basis $\sum_{k,s_o}(Y_{\text{TPM}} - \hat{Y}_{\text{TPM}}^{\text{sinc}})^2$	1,779.79	18.80×10^{-3}	50.00×10^{-3}	25.67×10^{-7}
Cubic *B-spline* $\sum_{k,s_o}(Y_{\text{TPM}} - \hat{Y}_{\text{TPM}}^{\text{spline}})^2$	38,958.51	41.16×10^{-2}	351.92	18.07×10^{-3}

Note: Sum of squared errors and mean squared errors (MSE) are computed among the four DSN data sets: modal, TPM, TPM with *sinc*, and TPM with *spline*. Time domain errors are computed directly from DSN data matrices while power spectral density (PSD) errors are computed from PSD estimates using Welch's method. DSN data matrices are $19 \times 4{,}982$.

Fig. 4 also compares measurements from mobile sensors 1, 10, and 19, computed by the TPM with *sinc* and cubic *spline* bases. The overall behavior of the mobile sensor data is captured well by both approximations. As quantified in Table 2, the *sinc* function outperforms the cubic spline in accuracy by an order of magnitude, with MSE equal to 18.80×10^{-3} versus 41.16×10^{-2}.

Fig. 5 displays the power spectral density (PSD) estimate, computed using the average of Welch's method over all 19 sensors. The data from the modal model and TPM contain nearly identical PSD estimates with MSE equal to 60.21×10^{-9}. Fig. 5 also provides the PSD estimate for the TPM data with those obtained using *sinc* and cubic *spline* basis approximations. The *sinc* PSD is coincident with previous TPM PSD, while the *spline* has, overall, less power. In Table 2, the approximation error is detailed, in which cubic *spline* MSE is four orders of magnitude higher than the MSE from *sinc*.

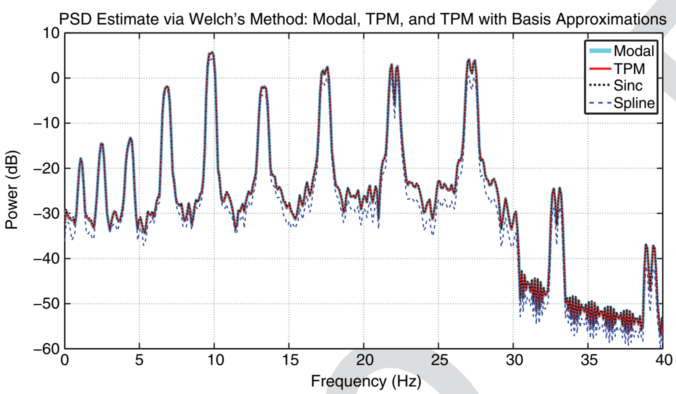

Fig. 5. Averaged PSD estimates of data from modal, TPM, and TPM with basis approximations computed via Welch's method for high-resolution mobile sensing application

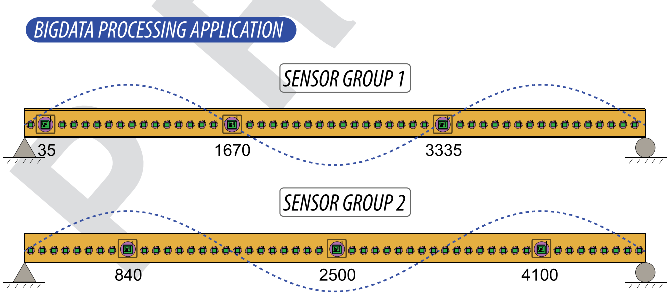

Fig. 6. BIGDATA processing application considers the switching between two groups; group 1 consists of sensing nodes 35, 1,670, and 3,335 while group 2 covers nodes 840, 2,500, and 4,100; the third-mode shape of the structure is superimposed to demonstrate the expected node responses to a third-mode harmonic excitation

BIGDATA Processing Application

In this subsection, the response of the simple beam, with modal properties given in Table 1, is measured using 5,000 sensors, one fixed at each sensing node. A harmonic load with frequency 2.45 Hz is applied at sensing node 2,500, resulting in an ideal forced, third-mode structural response. With responses available at 5,000 locations, the processing options are overwhelming. In this application, only three observations are considered in the offline DSN data set. Therefore, for the minimum model order, three modes are included in the TPM.

As pictured in Fig. 6, these observations are programmed to represent measurements in two specific sensing groups. Group 1 includes sensing nodes 35, 1,670, and 3,335, and group 2 includes sensing nodes 840, 2,500, and 4,100. The offline DSN matrix consists of data from group 1 until the 500th sample, when the observations switch to group 2. Clearly, this selection only represents one possible subset out of the many possibilities given in the BIGDATA population. Moreover, as pictured in Fig. 6, responses in group 1 are expected to be very small in magnitude due to the proximity of the nodes to zero-valued third-mode ordinates, and thus contain little information. When group 2 is selected, the responses are expected to have large values as the sensing nodes coincide with maximal third-mode ordinates.

As in the high-resolution mobile sensing application, the modal model, TPM, TPM with *sinc* bases, and TPM with cubic *splines* are considered to simulate the offline DSN data set. The DSN data are compared in time and frequency domain.

BIGDATA Results

In Fig. 7, a plot of each observation is provided along relevant node responses to display the observation switching scheme. For example, in Fig. 7(a), observation 1 is shown with nodes 35 and 840 for all samples. During samples 1 through 499, sensing group 1 is active, so that observation 1 represents samples at node 35. During samples 500 through 1,000, sensing group 2 is active and observation 1 represents samples at node 840. Figs. 7(b and c) show a parallel relationship with observation 2 and nodes 1,670 and 2,500, as well as observation 3 and nodes 3,335 and 4,100.

Fig. 8 provides the true DSN values computed using the modal and TPM. TPM approximations with *sinc* and cubic *spline* basis are also included. As mentioned previously, the modal and TPM data sets are theoretically exact, so the only differences are computational as indicated with an MSE equal to 46.54×10^{-6} in Table 3. The *sinc* and *B-spline* approximations capture the overall behavior; however, the superior accuracy of sinc basis is evident. Quantitatively, the MSE for the *sinc* approximation is two orders of magnitude lower than that of the cubic *B-spline*.

In Fig. 9, the PSD estimates are plotted for all four models. Consistent with previous analyses, the overall behavior of the response is captured by all four models. The modal model, TPM, and TPM with *sinc* basis approximation are all in agreement, while there is overall considerably less power in the *B-spline* approximation.

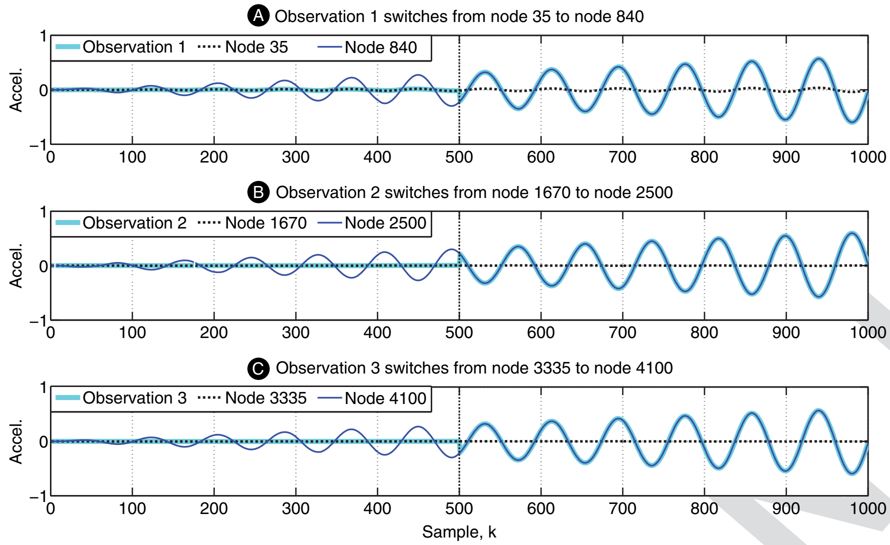

Fig. 7. Each observation of the offline DSN data matrix is plotted with relevant sensor node responses as scheduled in the BIGDATA application; group switching occurs at sample 500: (a) observation 1 with responses at nodes 35 and 840; as scheduled in the BIGDATA application, observation 1 switches from sensing node 35 to 840; (b) observation 2 with responses at nodes 1,670 and 2,500; (c) observation 3 with responses at nodes 3,335 and 4,100

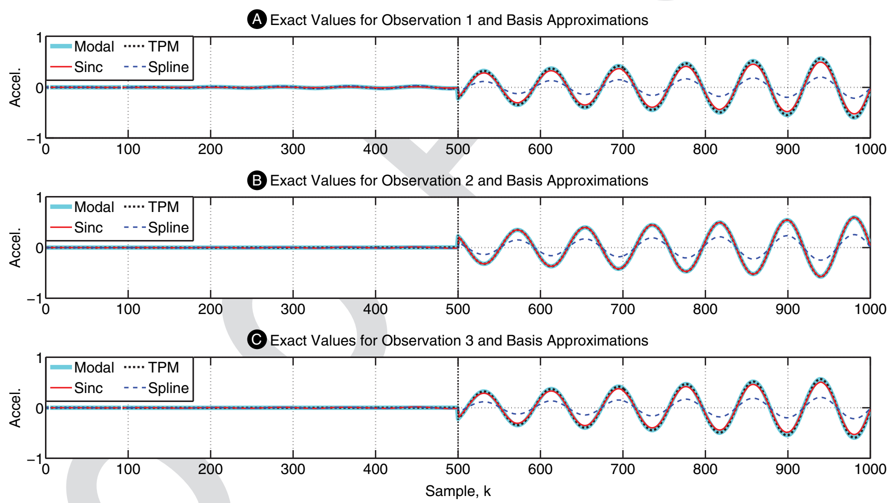

Fig. 8. (a) Modeled BIGDATA offline DSN observation 1 computed using the modal model, TPM, and TPM with basis approximations; (b) the modeled BIGDATA offline DSN observation 2 computed using the modal model, TPM, and TPM with basis approximations; (c) modeled BIGDATA offline DSN observation 3 computed using the modal model, TPM, and TPM with basis approximations

Table 3. Comparison of Offline DSN Data in BIGDATA Application

Error type	Sum of squares in time domain	Time domain MSE	Sum of squares of PSD	PSD MSE
Computational $\sum_{k,s_o}(Y_{\text{modal}} - Y_{\text{TPM}})^2$	13.96×10^{-2}	46.54×10^{-6}	11.17×10^{-9}	28.87×10^{-12}
Sinc basis $\sum_{k,s_o}(Y_{\text{TPM}} - \hat{Y}_{\text{TPM}}^{\text{sinc}})^2$	1.61	53.81×10^{-5}	16.82×10^{-5}	43.46×10^{-8}
Cubic *B-spline* $\sum_{k,s_o}(Y_{\text{TPM}} - \hat{Y}_{\text{TPM}}^{\text{spline}})^2$	61.50	20.50×10^{-3}	38.84×10^{-4}	10.04×10^{-6}

Note: Sum of squared errors and mean squared errors (MSE) are computed among the four DSN data sets: modal, TPM, TPM with *sinc*, and TPM with *spline*. Time domain errors are computed directly from DSN data matrices while power spectral density (PSD) errors are computed from PSD estimates using Welch's method. DSN data matrices are $3 \times 1{,}000$.

However, in this case, the computational PSD MSE is 28.87×10^{-12} and the *sinc* approximation PSD MSE is 43.46×10^{-8}, two orders of magnitude lower than the *B-spline* PSD MSE. The accuracy of the *spline* MSR approximation can be improved by including additional modes in the model. In the previous application where 19 modes were considered, there was little discrepancy between the TPM with a *spline* basis and the TPM with a *sinc* basis. Thus, when the number of modes included in the TPM is

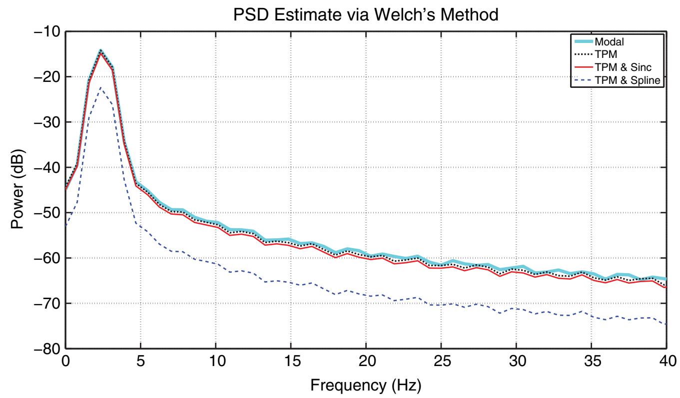

Fig. 9. Averaged PSD estimates of TPM data and basis approximations, computed via Welch's method for BIGDATA processing application

small or moderate, the *sinc* basis is recommended to approximate the MSR term.

While this application utilized many sensors to capture a simple response, it is clear that observation switching through offline DSN provides a powerful technique for generating aggregate data sets with dense structural information. For example, an optimal sensor network strategy (Chang and Pakzad 2014; Guo et al. 2004; Papadimitriou 2004) could be implemented to extract an optimal (by some measure) offline DSN data matrix from an available fixed sensor network, perhaps, a BIGDATA population. Moreover, in general, the goal is to use this strategy to build smart DSN data sets, which carry rich structural information in a compact size.

Conclusions

In this paper, dynamic sensor network (DSN) data sets were proposed to efficiently store measurements from a very large quantity of sensing nodes in a relatively small matrix. Note that a physical DSN system is not required to obtain a DSN data matrix. Spatial discontinuities in DSN data matrices enable a high capacity for storing spatial information. In the section "Dynamic Sensor Network Data" the concept of DSN was formally introduced and the roles of sensors, sensing nodes, and observations were defined. General types of DSN, such as online and offline, were also established.

In the section "Exact State-Space Models for Dynamic Sensor Networks" classical state-space models were modified to represent DSN data sets and associated modeling challenges were identified. Primarily, in the standard state-space model, the state variable coincides with sensing nodes; thus, a dense spatial grid dictates an overly complex dynamic model. The truncated physical model (TPM) was proposed as a computationally efficient technique to address these challenges. The TPM is theoretically equivalent to a modal state-space model with DSN observations (presented earlier in this paper) and establishes an intuitive relationship between the observation size of the DSN data matrix and the complexity of the underlying dynamic states. Additional benefits of the TPM include an unrestricted physical state variable, which represents user-defined *virtual probing locations* (VPL); in other words, the user may choose which sensing nodes define the state variable. This is a vast improvement on the coupled nature between states and sensing nodes seen in the standard state-space model.

In the section "Mode Shape Regression Using Basis Functions" the approximation of the *mode shape regression* term, defined in Eq. (34) of the TPM, through basis functions is discussed. Using the Whitaker-Kotelnikov-Shannon (WKS) reconstruction theory, *sinc* or *spline* bases are implemented in the TPM to bypass additional mode shape matrices in the observation equation. The result simplifies the subsequent system identification of TPM by eliminating the complex linear parameter varying (LPV) nature of the model, thus avoiding LPV-type identification algorithms.

High-resolution mobile sensing and BIGDATA processing applications were considered in the section "Processing Data from Novel Sensing Techniques" to exemplify novel sensing explorations with DSN data. In high-resolution mobile sensing, information from the responses at 5,000 sensing nodes was measured by 19 moving sensors and condensed into a 19×1 vector at each sample, and modeled with a 38×1 state variable. Note theoretically, in the standard state space model, the state variable would be restricted to a $10{,}000 \times 1$ vector. The BIGDATA processing application demonstrated the versatility in offline DSN data sets and the ability to process a smart subset. Given a very dense fixed sensor array and an enormous data matrix, offline DSN provide the ability to build an information-packed data matrix from user-selected sensor measurements. In the application, the second sensor group contained significantly more structural information than the first sensor group, exhibiting the utility in offline DSN for processing BIGDATA.

Acknowledgments

Research funding is partially provided by the National Science Foundation through Grant No. CMMI-1351537 by Hazard Mitigation and Structural Engineering program, and by a grant from the Commonwealth of Pennsylvania, Department of Community and Economic Development, through the Pennsylvania Infrastructure Technology Alliance (PITA).

Notation

The following symbols are used in this paper:

A = standard state matrix; size is $pN \times pN$;

A_c = continuous-time state matrix of the standard state-space model; size is $pN \times pN$;

$A^{\langle M \rangle}$ = modal state matrix; size is $pM \times pM$ and $M \ll N$;

$A_c^{\langle M \rangle}$ = continuous-time state matrix of the modal state-space model; size is $pM \times pM$ and $M \ll N$;

A^* = TPM state matrix; size is $pN_\alpha \times pN_\alpha$ and $N_\alpha = N_O = M$;

B = standard state input matrix; size is $pN \times N$;

B_c = continuous-time state matrix of the standard state-space model; size is $pN \times N$;

$B^{\langle M \rangle}$ = modal state input matrix; size is $pM \times M$ and $M \ll N$;

$B_c^{\langle M \rangle}$ = continuous-time state matrix of the modal state-space model; size is $pM \times M$ and $M \ll N$;

B^* = TPM state input matrix; size is $pN_\alpha \times N_\alpha$ and $N_\alpha = N_O = M$;

B_f = scaling matrix for the applied forces in the continuous-time equation of motion; size is $N \times N$

$\bar{C}$ = modal damping matrix for M modes; size is $M \times M$ and $M \ll N$;

C = standard observation matrix; size is $N_O \times pN$;

C_a = measurement conversion matrix, as described in section 7.2.1 of Juang and Phan 2001; size is $N_O \times N_O$

$C^{\langle M \rangle}$ = modal observation matrix; size is $M \times pM$ and $M \ll N$;

$C_a^{\langle M \rangle}$ = modal measurement conversion matrix; size is $M \times M$;
C^* = TPM observation matrix; size is $M \times pN_\alpha$ and $N_\alpha = N_O = M$;
$\bar{c}$ = structural damping matrix for N DOF; size is $N \times N$;
K = number of time samples (number of rows in DSN data matrix); scalar;
$\bar{K}$ = modal stiffness matrix for M modes; size is $M \times M$ and $M \ll N$;
$\bar{k}$ = structural stiffness matrix for N DOF; size is $N \times N$;
k = time step index;
M = number of modes included in analysis; scalar;
$\bar{M}$ = modal mass matrix for M modes; size is $M \times M$ and $M \ll N$;
$\bar{m}$ = structural mass matrix for N DOF; size is $N \times N$;
m = mode index;
N = total number of sensing nodes in model (DOF); scalar;
N_O = observation size (number of columns in DSN data matrix); scalar;
N_{mc} = number of sensors (measurement channels) in data set; scalar;
n = degree of *B-spline* Ω_{spline}; scalar;
N_χ = total number of sensing nodes in subset χ;
N_α = total number of VPL, i.e., sensing nodes in subset α;
N_δ = total number of sensing nodes in subset δ;
O = spatial subset corresponding to observations; when the observations are DSN data, this is a time-variant function, i.e., $O = O(k)$;
p = state-space model order (theoretically, $p = 2$); scalar;
$p_k^{\langle m \rangle}$ = modal input for mode m at time step k;
$q_k^{\langle m \rangle}$ = modal displacement for mode m at time step k;
$\dot{q}_k^{\langle m \rangle}$ = modal velocity for mode m at time step k;
$\ddot{q}_k^{\langle m \rangle}$ = modal acceleration for mode m at time step k;
S_O = sensor-position matrix for observations; size is $K \times N_O$
$\mathbf{s}$ = vector describing locations of all sensing nodes; size is $N \times 1$;
$\Delta \mathbf{s}_i$ = spacing for a uniform sensing node subset $\mathbf{s}_i$;
$\mathbf{s}_i$ = vector describing locations of sensing nodes in subset i; size is $N_i \times 1$;
T = coordinate transformation from modal to truncated physical coordinates; size is $pN_\alpha \times pM$ and $N_\alpha = N_O = M$;
$\mathbf{u}_k(\mathbf{s}_i)$ = vector of displacement responses at $\mathbf{s}_i$ and time step k;
$\dot{\mathbf{u}}_k(\mathbf{s}_i)$ = vector of velocity responses at $\mathbf{s}_i$ and time step k;
$\ddot{\mathbf{u}}_k(\mathbf{s}_i)$ = vector of acceleration responses at $\mathbf{s}_i$ and time step k;
$\mathbf{w}_k$ = sensor noise at time step k;
$\mathbf{x}_k$ = standard state vector at time step k; size is $pN \times 1$;
$\mathbf{x}_k^*$ = TPM state vector at time step k; size is $pN_\alpha \times 1$ and $N_\alpha = N_O = M$;
$\mathbf{y}_k$ = observation vector at time-step k (transposed row of DSN data); size is $N_O \times 1$;
$\mathbf{z}_k$ = modal state vector at time-step k; size is $pM \times 1$ and $M \ll N$;
α = spatial subset corresponding to VPL; individually indexed as $\alpha_1, \ldots, N_\alpha$;
$\beta^n(\,)$ = *B-spline* function with degree n;
χ = uniformly spaced sensing node subset; individually indexed as $\chi_1, \ldots, N_\chi$;
δ = general sensing node subset; individually indexed as $\delta_1, \ldots, N_\delta$;
Φ = mode shape matrix for M modes at all sensing nodes; also known as $\Phi^{\langle M \rangle}(\mathbf{s})$; size is $N \times M$;
Δt = sampling period in seconds;
Φ_i = mode shape matrix for M modes at sensing nodes in subset i; also known as $\Phi^{\langle M \rangle}(\mathbf{s}_i)$; size is $N_i \times M$;
$\boldsymbol{\eta}_k$ = forcing function at time-step k; size is $N \times 1$;
$\boldsymbol{\upsilon}_k$ = modal input at time-step k; size is $M \times 1$ and $M \ll N$;
Ω = TPM mode shape regression term; size is $N_O \times M$ and $M = N_O$;
Ω_{sinc} = *sinc* basis estimate for mode shape regression term; size is $N_O \times M$ and $M = N_O$; and
Ω_{spline} = *B-spline* estimate of degree n for mode shape regression term; size is $N_O \times M$ and $M = N_O$.

References

Abdel-Ghaffar, A., and Scanlan, R. H. (1985). "Ambient vibration studies of Golden Gate Bridge: 1. Suspended structure." *J. Eng. Mech.*, 10.1061/(ASCE)0733-9399(1985)111:4(463), 463–482.

Abdel-Ghaffar, A. M. (1976). "Dynamic analyses of suspension bridge structures." *Final Rep. No. EERL-76-01*, Earthquake Engineering Research Laboratory, California Institute of Technology, Pasadena, CA.

Aldroubi, A., Unser, M., and Eden, M. (1992). "Cardinal spline filters: Stability and convergence to the ideal sinc interpolator." *Signal Process.*, 28(2), 127–138.

Andersen, P., Brinker, R., Peeters, B., De Roeck, G., Hermans, L., and Krämer, C. (1999). "Comparison of system identification methods using ambient bridge test data." *Int. Modal Analysis Conf.*, 1035–1041.

Beutler, F. J. (1961). "Sampling theorems and bases in a Hilbert space." *J. Inf. Control*, 4(2), 97–117.

Beutler, F. J. (1966). "Error-free recovery of signals from irregularly spaced samples." *SIAM Rev.*, 8(3), 328–335.

Butzer, P. L., Engels, W., Ries, S., and Stens, R. L. (1986). "The Shannon sampling series and the reconstruction of signals in terms of linear, quadratic and cubic splines." *SIAM J. Appl. Math.*, 46(2), 299–323.

Carder, D. S. (1937). "Observed vibrations of bridges." *Bull. Seismol. Soc. Am.*, 27(4), 267–303.

Cerda, F., et al. (2012). "Indirect structural health monitoring in bridges: Scale experiments." *Proc., 7th Int. Conf. on Bridge Maintenance, Safety and Management*, Lago Di Como, 346–353.

Chang, M., and Pakzad, S. N. (2012). "Modified natural excitation technique for stochastic modal identification." *J. Struct. Eng.*, 10.1061/(ASCE)ST.1943-541X.0000559, 1753–1762.

Chang, M., and Pakzad, S. N. (2013). "Observer kalman filter identification for output-only systems using interactive structural modal identification toolsuite (SMIT)." *J. Bridge Eng.*, 19(5), 1–11.

Chang, M., and Pakzad, S. N. (2014). "Optimal sensor placement for modal identification of bridge systems considering number of sensing nodes." *J. Bridge Eng.*, 10.1061/(ASCE)BE.1943-5592.0000594, 04014019.

Chopra, A. K. (2007). *Dynamics of structures—Theory and applications to earthquake engineering*, Pearson, Prentice Hall, Upper Saddle River, NJ.

Dorvash, S., Pakzad, S., Naito, C., Hodgson, I., and Yen, B. (2014a). "Application of state-of-the-art in measurement and data analysis techniques for vibration evaluation of a tall building." *Struct. Infrastruct. Eng.*, 10(5), 654–669.

Dorvash, S., Pakzad, S. N., and Labuz, E. L. (2014b). "Statistics based localized damage detection using vibration response." *Smart Struct. Syst.*, 14(2), 85–104.

Gonzalez, A., O'Brien, E. J., and McGetrick, P. J. (2012). "Identification of damping in a bridge using a moving instrumented vehicle." *J. Sound Vib.*, 331(18), 4115–4131.

Guo, H. Y., Zhang, L., Zhang, L. L., and Zhou, J. X. (2004). "Optimal placement of sensors for structural health monitoring using improved genetic algorithms." *Smart Mater. Struct.*, 13(3), 528–534.

Inaudi, D., and Glisic, B. (2010). "Long-range pipeline monitoring by distributed fiber optic sensing." *J. Press. Vessel Technol.*, 132(1), 011701.

Jagerman, D. L., and Fogel, L. J. (1956). "Some general aspects of the sampling theorem*." *IRE Trans. Inf. Theory*, 2(4), 139–146.

Jerri, A. J. (1977). "Shannon sampling theorem—Its various extensions and applications: A tutorial review." *Proc. IEEE*, 65(11), 1565–1596.

Juang, J.-N., and Pappa, R. S. (1984). "An eigensystem realization algorithm for modal parameter identification and model reduction." *NASA Langley Res. Center*, 8(5), 620–627.

Juang, J.-N., and Phan, M. Q. (2001). *Identification and control of mechanical systems*, Cambridge University Press, Cambridge, U.K.

Kotelnikov, W. A. (1933). "On the transmission capacity of the 'ether' and of cables in electrical communications." *Proc., 1st All-Union Conf. on the Technological Reconstruction of the Communications Sector and the Development of Low-Current Engineering*, Moscow.

Lei, Y., et al. (2003). "Statistical damage detection using time series analysis on a structural health monitoring benchmark problem." *Proc., 9th Int. Conf. on Applications of Statistics and Probability in Civil Engineering*, 6–9.

Lin, C. W., and Yang, Y. B. (2005). "Use of a passing vehicle to scan the fundamental bridge frequencies: An experimental verification." *Eng. Struct.*, 27(13), 1865–1878.

Matarazzo, T. J., and Pakzad, S. N. (2014). "Modal identification of Golden Gate Bridge using pseudo mobile sensing data with STRIDE." *Dynamics of Civil Structures*, Vol. 4, Springer, 293–298.

Matarazzo, T. J., and Pakzad, S. N. (2015a). "STRIDE for Structural identification using expectation maximization: Iterative output-only method for modal identification." *J. Eng. Mech.*, 10.1061/(ASCE)EM.1943-7889.0000951, in press.

Matarazzo, T. J., and Pakzad, S. N. (2015b). "Structural modal identification for mobile sensing with missing data." *J. Eng. Mech.*, 10.1061/(ASCE)EM.1943-7889.0001046, in press.

Matarazzo, T. J., Shahidi, S. G., Chang, M., and Pakzad, S. N. (2015a). "Are today's SHM procedures suitable for tomorrow's BIGDATA?" *Structural Health Monitoring and Damage Detection*, Vol. 7, Springer, 59–65.

Matarazzo, T. J., Shahidi, S. G., and Pakzad, S. N. (2015b). "Exploring the efficiency of BIGDATA analyses in SHM" *Proc., 10th Int. Workshop on Structural Health Monitoring*, DEStech, Toronto, ON, Canada.

McGetrick, P. J., González, A., and O'Brien, E. J. (2009). "Theoretical investigation of the use of a moving vehicle to identify bridge dynamic parameters." *Insight—Non-destructive testing and condition monitoring*, 51(8), 433–438.

McLamore, V. R., Hart, G. C., and Stubbs, I. R. (1971). "Ambient vibration of two suspension bridges." *J. Struct. Div.*, 97(10), 2567–2582.

Moheimani, S. O. R., Halim, D., and Fleming, A. J. (2003). *Spatial control of vibration: Theory and experiments*, A. Guran, C. Christov, M. Cloud, F. Pichler, and W. B. Zimmerman, eds., World Scientific, Singapore.

Oppenheim, A. V., Schafer, R. W., and Buck, J. R. (1999). *Discrete-time signal processing*, Prentice-Hall, Upper Saddle River, NJ.

Pakzad, S. N., and Fenves, G. L. (2009). "Statistical analysis of vibration modes of a suspension bridge using spatially dense wireless sensor network." *J. Struct. Eng.*, 10.1061/(ASCE)ST.1943-541X.0000033, 863–872.

Pakzad, S. N., Fenves, G. L., Kim, S., and Culler, D. E. (2008). "Design and implementation of scalable wireless sensor network for structural monitoring." *J. Infastruct. Syst.*, 10.1061/(ASCE)1076-0342(2008)14:1(89), 89–101.

Papadimitriou, C. (2004). "Optimal sensor placement methodology for parametric identification of structural systems." *J. Sound Vib.*, 278(4–5), 923–947.

Peeters, B., and De Roeck, G. (1999). "Reference-based stochastic subspace identification for output-only modal analysis." *Mech. Syst. Signal Process.*, 13(6), 855–878.

Rainer, J. H., and Selst, V. A. (1976). "Dynamic properties of Lions' Gate suspension bridge." *ASCE/EMD Specialty Conf.: Dynamic Response of Structures: Instrumentation, Testing Methods, and System Identification*, Los Angeles, CA, 243–252.

Shahidi, S. G., Pakzad, S. N., Ricles, J. M., Martin, J. R., Olgun, C. G., and Godfrey, E. A. (2015). "Behavior and damage of the Washington monument during the 2011 Mineral, Virginia, earthquake." *Geol. Soc. Am.*, 2509(13), 235–252.

Shannon, C. E. (1998). "Communication in the presence of noise." *Proc. IEEE*, 86(2), 447–457.

Smyth, A., and Wu, M. (2007). "Multi-rate Kalman filtering for the data fusion of displacement and acceleration response measurements in dynamic system monitoring." *Mech. Syst. Sig. Process.*, 21(2), 706–723.

Smyth, A. W., Pei, J.-S., and Masri, S. F. (2003). "System identification of the Vincent Thomas suspension bridge using earthquake records by system identification of the Vincent Thomas suspension bridge using earthquake records." *Earthquake Eng. Struct. Dyn.*, 32(3), 339–367.

Stenger, F. (1976). "Approximations via Whittaker's cardinal function." *J. Approx. Theory*, 17(3), 222–240.

Trifunac, M. D. (1970). "Wind and microtremor induced vibrations of a twenty-two story steel frame building." *Final Rep. No. EERL-70-02*, Earthquake Engineering Research Laboratory, California Institute of Technology, Pasadena, CA.

Unser, M. (1999). "Splines: A perfect fit for signal and image processing." *IEEE Signal Process. Mag.*, 16(6), 22–38.

Vincent, G. S. (1962). "Golden Gate Bridge vibration studies." *Trans. ASCE*, 127(2), 667–707.

Whittaker, E. T. (1915). "On the functions which are represented by the expansions of interpolation-theory." *Proc. Roy. Soc. Edinburgh*, 35(1915), 181–194.

Whittaker, J. M. (1928). "The 'Fourier' theory of the cardinal function." *Proc. Edinburgh Math. Soc.*, 1(3), 169–176.

Yang, Y.-B., Lin, C. W., and Yau, J. D. (2004). "Extracting bridge frequencies from the dynamic response of a passing vehicle." *J. Sound Vib.*, 272(3–5), 471–493.

Zhu, D., Guo, J., Cho, C., Wang, Y., and Lee, K. (2012). "Wireless mobile sensor network for the system identification of a space frame bridge." *IEEE/ASME Trans. Mechatron.*, 17(3), 499–507.